JACS
JOURNAL OF THE AMERICAN CHEMICAL SOCIETY
Article
pubs.acs.org/JACS

Prediction of Silicon-Based Layered Structures for Optoelectronic Applications

Wei Luo,[†] Yanming Ma,[‡] Xingao Gong,[†,§] and Hongjun Xiang*,[†,§]

[†]Key Laboratory of Computational Physical Sciences (Ministry of Education), State Key Laboratory of Surface Physics, and Department of Physics, Fudan University, Shanghai 200433, P. R. China

[§]Collaborative Innovation Center of Advanced Microstructures, Fudan University, Shanghai 200433, P. R. China

[‡]State Key Lab of Superhard Materials, Jilin University, Changchun 130012, China

Supporting Information

ABSTRACT: A method based on the particle swarm optimization algorithm is presented to design quasi-two-dimensional materials. With this development, various single-layer and bilayer materials of C, Si, Ge, Sn, and Pb were predicted. A new Si bilayer structure is found to have a more favored energy than the previously widely accepted configuration. Both single-layer and bilayer Si materials have small band gaps, limiting their usages in optoelectronic applications. Hydrogenation has therefore been used to tune the electronic and optical properties of Si layers. We discover two hydrogenated materials of layered Si_8H_2 and Si_6H_2 possessing quasidirect band gaps of 0.75 and 1.59 eV, respectively. Their potential applications for light-emitting diode and photovoltaics are proposed and discussed. Our study opened up the possibility of hydrogenated Si layered materials as next-generation optoelectronic devices.

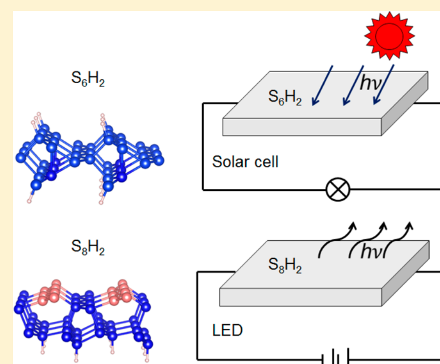

■ INTRODUCTION

In recent years, two-dimensional (2D) or quasi-two-dimensional (Q2D) materials have attracted much interest for their fascinating properties. Graphene, a single-layer of carbon atoms with honeycomb configuration, has been widely studied[1−4] due to its novel Dirac-like electronic properties. It has rapidly become a candidate for the next generation of faster and smaller electronic devices. Besides graphene, other layered materials[5−7] with excellent properties were also discovered. Monolayer MoS_2 with a direct band gap[8,9] can be used to construct interband tunnel field-effect transistors (FET),[10] which have lower power consumption than classical transistors. Recently, few-layer black phosphorus crystals with thickness down to a few nanometers have been fabricated. Researchers show that it is also a good material for fabricating FET.[5] Coleman et al.[11] reported that a variety of inorganic layered materials can be obtained through a straightforward liquid exfoliation technique.

Due to the high stability, high abundance, and the existence of an excellent compatible oxide (SiO_2), Si is the leading material for microelectronic devices. Because of the excellent compatibility with the mature Si-based microelectronics industry and high abundance of Si, Si-based layered materials may be the most promising layered materials for realistic applications. Although the majority of solar cells fabricated to date have been based on three-dimensional (3D) bulk diamond Si,[12] it is well-known that 3D bulk Si is not an ideal material for optoelectronic applications because Si is an indirect band gap (1.1 eV) semiconductor and there is a large energy difference between the direct gap (3.4 eV) and the indirect gap.[13] Thus, the discovery of Si-based layered materials with excellent optoelectronic properties might lead to revolution in future optoelectronics technology.

Like graphene, single-layer Si has a honeycomb structure with the linear dispersion of the band structure near the Dirac point.[14−19] Moreover, it was identified as a topological insulator[20,21] (TI) with a tiny band gap (1.55 meV), which is too small for optoelectronic applications. At the same time, single-layer silicene itself is unstable. It must be grown on metallic substrates[22,23] and cannot be exfoliated from substrates. Furthermore, substrates change the electronic properties of silicene.[24−26] Thus, it is highly desirable to discover new, free-standing, stable, Si-based layered materials with exceptional optoelectronic properties.

In our work, we propose a new general global optimization method to predict Q2D structures based on the particle swarm optimization (PSO) technique as implemented in the CALYPSO (crystal structure analysis by particle swarm optimization) code.[27,28] With this development, a new Si bilayer structure with lower energy than the widely accepted lowest energy configuration has been predicted. Furthermore, we find two layered structures, namely, Si_8H_2-*Pm*11 and Si_6H_2-*Pmm*2. They have quasi-direct gaps of 0.75 and 1.59 eV, respectively. These new structures are promising candidates for optoelectronic applications.

Received: July 15, 2014
Published: October 14, 2014

 © 2014 American Chemical Society

COMPUTATIONAL METHODS

PSO Algorithm for the Q2D System. PSO is designed to solve problems related to multidimensional optimization,[29] which is inspired by the social behavior of birds flocking or fish schooling. Recently, the PSO algorithm was adopted to successfully predict 3D crystal structure as implemented in the CALYPSO code.[27,28] Previously, we proposed a modified PSO algorithm for predicting single-atom-thick planar 2D crystals, such as graphene and BN sheet.[7] This approach was subsequently extended to search multilayer structures.[30] In this later development, it requires the number of layers and number of atoms in each layer as the input[30] when searching a multilayer Q2D structure. However, this information is not always known prior to the search of a new Q2D system, which limits its usage. Here, we propose a more general way to predict Q2D systems based on the PSO algorithm.[27] With this development, prediction of Q2D materials without specifying the number of layers and the chemical composition per layer becomes feasible.

In our implementation, we generate random Q2D structures with the thickness along the *c*-axis smaller than a given thickness *d*. We note that specifying the thickness *d* in the structure searching is more general and unambiguous than specifying the number of layers. A Q2D crystal can be characterized by 80 layer space groups, different from the planar 2D crystals characterized by 17 planar space groups. To generate a random Q2D structure, we first randomly select a layer group. The lateral lattice parameters and atomic positions are then randomly generated but confined within the chosen layer group symmetry. The generation of random structures ensures unbiased sampling of the energy landscape. The explicit application of symmetric constraints leads to significantly reduced search space and optimization variables and thus hastens global structural convergence. Subsequently, local optimization, including that of the atomic coordinates and lateral lattice parameters, is performed for each of the initial structures. In the next generation, a certain number of new structures (the best 60% of the population size) are generated by PSO. The other structures are generated randomly, which is critical to increase the structure diversity. Within the PSO scheme,[27] a structure in the searching phase space is regarded as a particle. A set of particles (structures) is called a population or a generation. The positions of the particle are updated according to the following equation

$$x_{i,j}^{t+1} = x_{i,j}^{t} + v_{i,j}^{t+1}$$

where x and v are the position and velocity, respectively [i is the atom index, and j refers to the dimension of the structure ($1 \leq j \leq 3$) and is the generation index]. The new velocity of each particle is calculated on the basis of its previous location ($x_{i,j}^t$) before optimization, previous velocity ($v_{i,j}^t$), current location (pbest$_{i,j}^t$) with an achieved best fitness (i.e., lowest energy), and the population global location (gbest$_{i,j}^t$) with the best fitness value for the entire population

$$v_{i,j}^{t+1} = wv_{i,j}^{t} + c_1 r_1(\text{pbest}_{i,j}^{t} - x_{i,j}^{t}) + c_2 r_2(\text{gbest}_{i,j}^{t} - x_{i,j}^{t})$$

where ω (in the range of 0.9−0.4) denotes the inertia weight, $c_1 = 2$ and $c_2 = 2$, and r_1 and r_2 are two separately generated random numbers uniformly distributed in the range [0, 1]. The initial velocity is generated randomly. All the structures produced by the PSO operation are then relaxed to the local minimum. When we obtain the new Q2D structure by the PSO operation or random generation, we make sure that the thickness of the Q2D structure is smaller than the given thickness *d*. Usually, tens of iterations are simulated to make sure that the lowest-energy structures are found.

To test the efficiency of this new method, we search some known Q2D systems. We set the population size to 30 and the number of generations to 20. Without giving any prior structure information except for the whole chemical composition, we find the known structures for layered MoS_2, GaS, and Bi_2Se_3 within 3, 2, and 11 generations, respectively. These tests indicate that our approach and its implementation are efficient.

In our simulation for the silicon-based Q2D systems, the total number of atoms is fixed to be no more than 12 in the unit cell. We only consider an even number of atoms, since many tests show that systems with an odd number of atoms usually have higher total energy. We consider five different thickness *d* (usually between 1 and 5 Å) for each system. In addition, we repeat twice of each calculation in order to make results reliable.

DFT Calculations. In this work, a density functional theory (DFT) method is used for structural relaxation and electronic structure calculation. The ion−electron interaction is treated by the projector augmented-wave (PAW[31]) technique, which is performed in the Vienna ab initio simulation package (VASP[32]). In the DFT plane-wave calculations, we use the local density approximation (LDA[33,34]). The 2D *k*-mesh is generated by the Monkhorst−Pack scheme, which depends on the lattice constant. For relaxed structures, the atomic forces are less than 0.01 eV/Å. To avoid interactions between different quasi-*ab*-planes, we set the vacuum thickness to 12 Å. As we know, LDA underestimates the band gap, so we adopt the HSE06 functional to calculate the electronic and optical properties.[35] To make sure of the dynamical stability of the obtained structures, we use the finite displacement method[36] as implemented in the PHONOPY code[37] to calculate the phonon frequencies.

RESULTS AND DISCUSSION

We predict the single-layer and bilayer structures of the silicon-related group IV elements systematically. Our results are listed in Table 1.

Table 1. Single-Layer and Bilayer Structures of Si, Ge, Sn, and Pb Predicted from Our Global Structure Optimizations

element	layer number	energy[a] (eV)	thickness (Å)	configuration[b]	property
Si	1	−5.2265	0.442	silicene	TI
	2	−5.4960	2.249	Si-*Cmme*	metal
Ge	1	−4.5215	0.624	silicene-like	TI
	2	−4.7281	2.405	Ge-*Cmme*	metal
Sn	1	−3.8454	0.806	silicene-like	TI
	2	−4.1785	2.600	Sn-$P\bar{3}m1$	metal
Pb	1	not stable[c]			
	2	−4.0523	2.603	Pb-$P\bar{3}m1$	metal

[a]The total energy is calculated by using LDA. [b]Some configurations (i.e., *Cmme*, $P\bar{3}m1$) are shown in Figures 1a and 2. [c]There are no dynamically stable single-layer Pb structures.

Single-Layer and Bilayer Si. If the thickness is less than the radius[38] of the element, we call it a single-layer structure. For single-layer Si, our results agree with a previous report.[20] It is the honeycomb silicene structure with a buckling of about 0.442 Å. Moreover, silicene is a TI in which the quantum spin Hall effect (QSHE) may be realized.[20] For bilayer Si, it is widely accepted that the AA stacking configuration (shown in Figure 1b and referred to as AA-Si) is the most stable structure.[39] Recently, Gimbert et al.[40] reported that Q2D Si may form the MoS_2-type structure. However, its total energy seems too high to be synthesized experimentally. From our PSO simulation, we find a new bilayer structure of Si with the layer group *Cmme*, namely, Si-*Cmme*. The LDA total energy of Si-*Cmme* is lower than that of AA-Si by 41 meV/atom. We also use the Perdew−Burke−Ernzerhof (PBE[41]) exchange−correlation function to calculate the total energy and find similar results. From Figure 1a,b, we can easily see that AA-Si has C_3 rotational symmetry, while the C_3 symmetry is broken in the Si-*Cmme*. Neither of these two structures has buckling. The simulated occupied STM images (Figure 1c,d) of Si-*Cmme* and AA-Si indicate that our prediction of the Si-*Cmme* structure may be easily confirmed by the STM experiment.

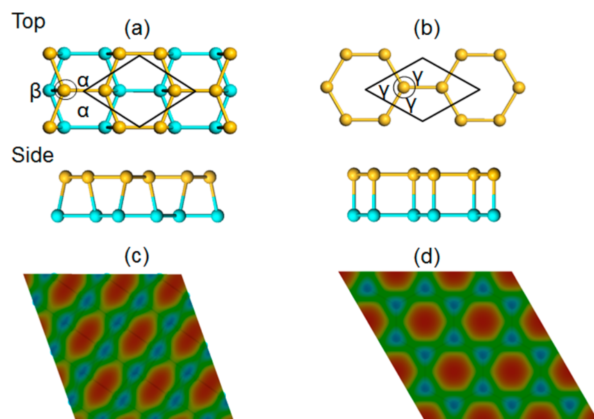

Figure 1. (a) Top and side views of Si-*Cmme*. (b) Top and side views of AA-Si. (c) The simulated occupied STM image of Si-*Cmme*. (d) The simulated occupied STM image of AA-Si. $\alpha = 110.2°$, $\beta = 139.6°$, $\gamma = 120°$. The Si atoms of the top layer and those of the bottom layer are indicated by different colors. The STM images are obtained by summing up all the local density of states from −1.0 eV to the Fermi level. From part b, we can easily see that AA-Si has C_3 symmetry, different from the case of Si-*Cmme*. The lateral unit cell is denoted by the black lines.

We calculated the electronic structures of AA-Si and Si-*Cmme* with the HSE06 functional. Band structures are shown in Figure 4a,b. From Figure 4a, we find that AA-Si is an indirect semiconductor with a band gap of about 130 meV, in agreement with previous results.[39] However, Si-*Cmme* is metallic with large dispersions of the valence band maximum (VBM) and conduction band minimum (CBM) states. Taking the vacuum level as the reference, we find that the CBM of Si-*Cmme* is much lower (by almost 1.0 eV) than that of the AA-Si. This can be seen from the band edge positions when the AA-Si structure evolves into the Si-*Cmme* structure (see Figure S4 of the Supporting Information). It should be noted that the CBM of Si-*Cmme* is below the Fermi level and thus is occupied. This is in accord with the lower energy of the Si-*Cmme* phase. In addition, calculations show that Si-*Cmme* is dynamically and thermally stable (see the Supporting Information). Since each Si atom in the bilayer Si-*Cmme* is 4-fold coordinated, Si-*Cmme* is much more stable (by 270 meV/atom) than the single-layer silicene.

Single-Layer and Bilayer of Other Group Elements. For carbon, our results agree with a previous study[1] very well, so we do not list the results of C in Table 1. Like silicene, single-layer Ge and Sn have a honeycomb configuration and are TIs. The band gaps are larger than that of silicene, because the spin−orbit coupling is stronger than that in Si. For Pb, we find that there is no dynamically stable single-layer structure. Similar to bilayer Si, we find bilayer Ge also has the *Cmme* configuration which has a lower energy by 21 meV/atom than the AA-Ge bilayer structure. For bilayer Sn and bilayer Pb, the lowest structure belongs to the layer group $P\bar{3}m1$ (see Figure 2), which is different from the cases of Si and Ge. All these bilayer structures are found to be metallic.

Our above simulations show that both single-layer and bilayer Si structures are not suitable for the optical and electronic applications because both structures do not have an appropriate band gap. It was shown that chemical functionalization can be used to tune or modify the electronic and optical properties of 2D and Q2D systems.[39,42−45] In order to identify Q2D Si-based systems for optoelectronic applications, we

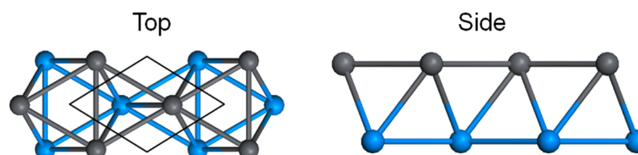

Figure 2. Top and side views of bilayer Sn-$P\bar{3}m1$ (Pb-$P\bar{3}m1$ is the same as Sn-$P\bar{3}m1$). The bilayer structure is formed by stacking two triangle layers.

performed a global search of hydrogenated Q2D Si structures. We consider four different compositions, i.e., Si_8H_2, Si_6H_2, Si_4H_2, and Si_4H_4.

Hydrogenate Si Layered Structure (Si_8H_2-*Pm*11). For Si_8H_2, we find that the lowest energy structure among all structures with thickness less than 6.0 Å is Si_8H_2-*Pm*11, as shown in Figure 3a. Similar to the proposed $Si_{24}H_6$ structure,[39]

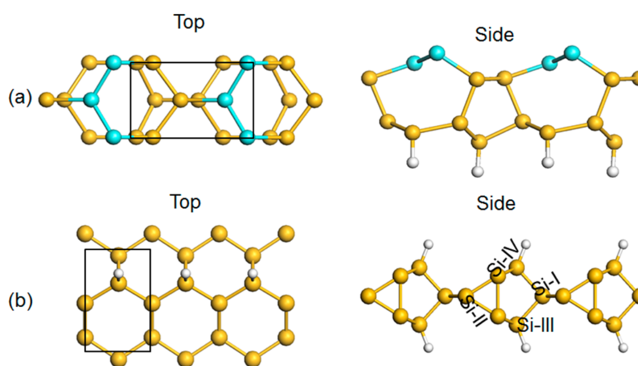

Figure 3. (a) The top and side views of Si_8H_2-*Pm*11. The 3- and 4-fold coordinated Si atoms are marked by aquamarine and yellow, respectively. These 3-fold coordinated Si atoms form a one-dimensional zigzag chain. (b) The top and side views of Si_6H_2-*Pmm*2. Each Si atom is 4-fold coordinated. For type-I, type-II, and type-IV Si atoms, all the four nearest neighbors are Si atoms. The type-III Si atom forms a covalent bond with one H atom. Two type-IV Si atoms and one type-II Si atom form a triangle.

the hydrogen atoms only absorb at the bottom side in Si_8H_2-*Pm*11. However, Si_8H_2-*Pm*11 has a lower energy by 73 meV/atom than the previously proposed structure.[39] Except for the two 3-fold coordinated Si atoms on the top surface, all the other Si atoms are 4-fold coordinated. The two 3-fold coordinated Si atoms form a one-dimensional zigzag chain. As can be seen from the band structure shown in Figure 4c, the direct band gap and indirect band gap are 0.75 and 0.70 eV, respectively, which is close to the optimal wavelength (1.55 μm ≈ 0.8 eV) for the optical fiber communications. From the band decomposed charge density (Figure 5a), we find that the VBM and CBM states are mainly contributed by the zigzag chain formed by the 3-fold coordinated Si atoms. Furthermore, we compute the imaginary part ε_2 of the dielectric function to find that the direct gap transition is dipole-allowed. This is expected since Si_8H_2-*Pm*11 belongs to the *Cm* point group and the transition between any two eigenstates of a *Cm* system is dipole-allowed. The optical transition near the band edge is found to be rather strong. This is because both VBM and CBM states are 1D-like, resulting in the Van Hove-like singularity in the density of state near the band edge. Our calculations show that Si_8H_2-*Pm*11 is dynamically and thermally stable (see the Supporting Information).

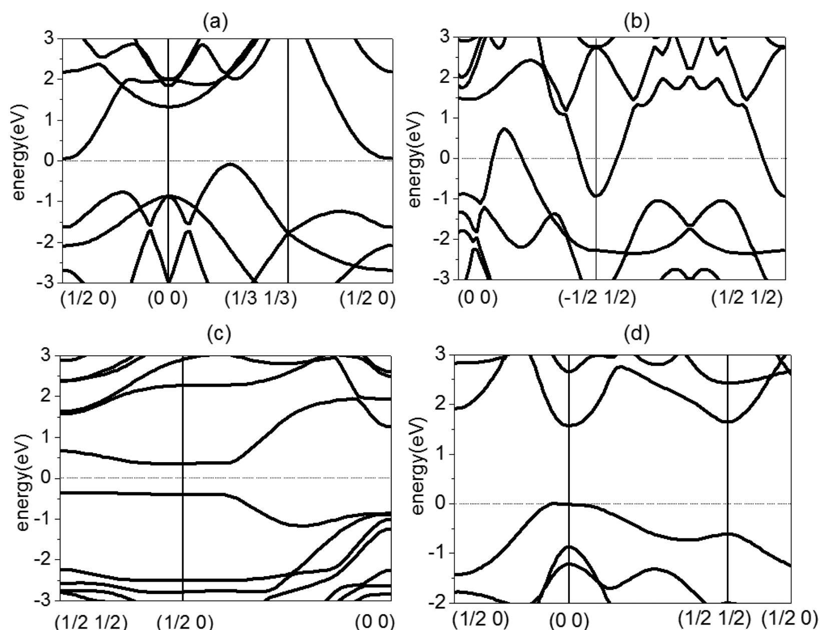

Figure 4. (a) Band structure of AA-Si from the HSE calculations. We can see that it is an indirect semiconductor with a very small band gap. (b) Band structure of Si-*Cmme*. Unlike AA-Si, it is a semimetal. (c) Band structure of Si_8H_2-*Pm*11. The VBM and CBM are almost flat along the direction that is perpendicular to the 1D zigzag chains formed by 3-fold coordinated Si atoms. (d) Band structure of Si_6H_2-*Pmm*2. It is a semiconductor with a quasidirect band gap of 1.59 eV.

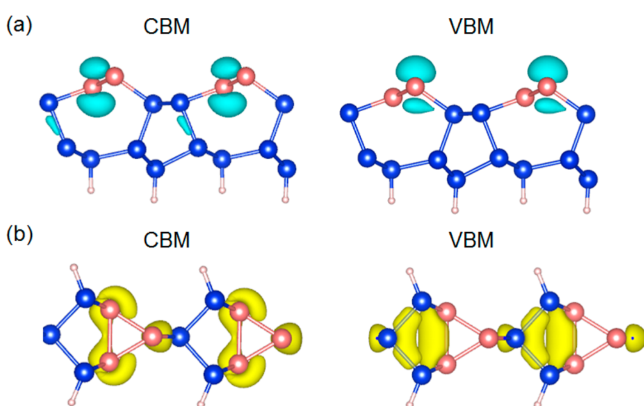

Figure 5. (a) The partial charge density of Si_8H_2-*Pm*11. Red atoms are 3-fold coordinate Si atoms. From this figure, we can see that the CBM and VBM states are mainly contributed by 3-fold coordinate Si atoms. (b) The partial charge density of Si_6H_2-*Pmm*2. Three 4-fold-coordinated red Si atoms form a triangle. Similar to Si_{20}, the band edge states distribute mainly around the Si triangle.

Hydrogenate Si Layered Structure (Si_6H_2-*Pmm*2). We find that the structure (i.e., Si_6H_2-*Pmm*2) shown in Figure 3b has the lowest energy among all Q2D structures with a thickness of less than 6.1 Å. In Si_6H_2-*Pmm*2, there are four different kinds of Si atoms. Each Si atom is 4-fold coordinated, indicating that this structure is highly stable. For type-I, type-II, and type-IV Si atoms, all the four nearest neighbors are Si atoms. The type-III Si atom forms a covalent bond with one H atom. The computed HSE06 band structure (Figure 4d) suggests that Si_6H_2-*Pmm*2 also has a quasidirect band gap. The direct band gap at Γ and indirect band gap are 1.59 and 1.52 eV, respectively, which is near the optimal value (about 1.5 eV) for solar-energy absorber applications. It is interesting to note that there is a Si triangle in Q2D Si_6H_2-*Pmm*2, similar to the predicted 3D structure of Si_{20}[46] with a quasidirect band gap near 1.5 eV. It appears that the presence of Si triangles is relevant to the desirable band gap value. The band decomposed charge density plot (Figure 5b) shows that the band edge states, in particular the CBM state, distribute mostly around the Si triangle. The computed imaginary part ε_2 of the dielectric function shows that the direct-gap transition in Si_6H_2-*Pmm*2 is dipole-allowed (see Figure 6). This can be easily understood by

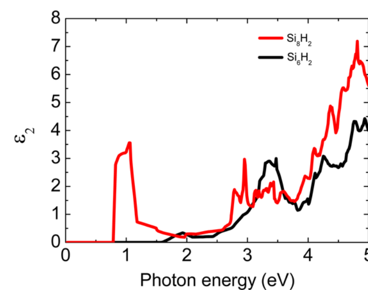

Figure 6. Imaginary part of the dielectric functions from the HSE06 calculations for Si_6H_2-*Pmm*2 and Si_8H_2-*Pm*11.

the group theory analysis. The point group of Si_6H_2-*Pmm*2 is C_{2v} with an in-plane 2-fold rotational axis. Detailed analysis shows that both the VBM and CBM states at Γ belong to the A_1 irreducible representation. Thus, the transition between the VBM and CBM states can be induced by a light with the electric field along the 2-fold rotational axis of the system. The good optical absorption and optimal direct gap suggest that Si_6H_2-*Pmm*2 is a good nanoscale solar cell absorber. The computed phonon frequencies (see the Supporting Information) indicate that Si_6H_2-*Pmm*2 is dynamically stable. Furthermore, molecular dynamics (MD) simulation indicates that it is thermally stable at least up to 800 K (see the Supporting Information).

Hydrogenate Si Layered Structure (Si_4H_2-*P*$\bar{3}$*m*1 and Si_4H_4-*Pman*). For Si_4H_2, we find that the lowest energy layered

structure is Si_4H_2-$P\overline{3}m1$, as shown in the Supporting Information. We can see that each Si atom is 4-fold coordinated, forming good sp^3 hybridization, which contributes to the large indirect band gap (about 2.1 eV) and low total energy. For Si_4H_4, it is widely accepted that the Si_4H_4 structure based on the silicene structure (Si_4H_4-$P\overline{3}m1$) is the most stable one. Here we find a new structure (Si_4H_4-*Pman*; see the Supporting Information) based on the black phosphorus structure that has a lower energy by about 4 meV/atom than that based on the silicene structure (see the Supporting Information).

From our simulations on hydrogenated Si layered structures, we find that the band gap tends to increase with the concentration of hydrogen because the Si atoms can form better sp^3 hybridization when there are more H atoms. Furthermore, we find that hydrogenation improves the thermal stability of the Si layered structures. For silicene and Si-*Cmme*, the melting points are about 500 and 600 K (see the Supporting Information). While for Si_8H_2-*Pm*11 and Si_6H_2-*Pmm*2, the melting points are about 800 and 900 K.

■ CONCLUSION

In summary, we have developed a new method based on the PSO algorithm to predict the Q2D crystal structure. Combining this method with first-principle calculations, we predict systematically the single-layer and bilayer structures of C, Si, Ge, Sn, and Pb. A new stack configuration of bilayer Si is revealed to have a lower energy than the previously known structures. Furthermore, we systematically search the hydrogenated Si layered structures, i.e., Si_8H_2, Si_4H_2, Si_6H_2, and Si_4H_4. In particular, we find that Si_8H_2-*Pm*11 and Si_6H_2-*Pmm*2 are stable and have desirable optical properties; thus, they are excellent candidates for generating light with optimal wavelength for the optical fiber communications and absorbing light in a solar cell, respectively.

■ ASSOCIATED CONTENT

Ⓢ Supporting Information

Phonon dispersions of Si-*Cmme*, Si_8H_2-*Pm*11, Si_6H_2-*Pmm*2; thermal stability of silicene, Si-*Cmme*, Si_8H_2-*Pm*11, Si_6H_2-*Pmm*2; lowest energy layered structure of Si_4H_2 and Si_4H_4; evolution of the CBM, VBM, and total energy from the AA-Si structure to the Si-*Cmme* structure; geometrical coordinates and energies for optimized structures; and complete ref 11. This material is available free of charge via the Internet at http://pubs.acs.org.

■ AUTHOR INFORMATION

Corresponding Author

hxiang@fudan.edu.cn

Notes

The authors declare no competing financial interest.

■ ACKNOWLEDGMENTS

Work was supported by NSFC, the Special Funds for Major State Basic Research, FANEDD, NCET-10-0351, Research Program of Shanghai Municipality and MOE, Program for Professor of Special Appointment (Eastern Scholar), and Fok Ying Tung Education Foundation.

■ REFERENCES

(1) Geim, A. K.; Novoselov, K. S. *Nat. Mater.* **2007**, *6*, 183.
(2) Novoselov, K. S.; Geim, A. K.; Morozov, S. V.; Jiang, D.; Katsnelson, M. I.; Grigorieva, I. V.; Dubonos, S. V.; Firsov, A. A. *Nature* **2005**, *438*, 197.
(3) Novoselov, K. S.; McCann, E.; Morozov, S. V.; Fal'ko, V. I.; Katsnelson, M. I.; Zeitler, U.; Jiang, D.; Schedin, F.; Geim, A. K. *Nat. Phys.* **2006**, *2*, 177.
(4) Zhang, Y. B.; Tan, Y. W.; Stormer, H. L.; Kim, P. *Nature* **2005**, *438*, 201.
(5) Li, L. K.; Yu, Y. J.; Guo, J. Y.; Ge, Q. Q.; Ou, X. D.; Wu, H.; Feng, D. L.; Chen, X. H.; Zhang, Y. B. *Nat. Nano.* **2014**, *9*, 372.
(6) Ataca, C.; Ciraci, S. *J. Phys. Chem. C* **2011**, *115*, 13303.
(7) Luo, X. Y.; Yang, J. H.; Liu, H. Y.; Wu, X. J.; Wang, Y. C.; Ma, Y. M.; Wei, S. H.; Gong, X. G.; Xiang, H. J. *J. Am. Chem. Soc.* **2011**, *133*, 16285.
(8) Mak, K. F.; Lee, C.; Hone, J.; Shan, J.; Heinz, T. F. *Phys. Rev. Lett.* **2010**, *105*, 136805.
(9) Splendiani, A.; Sun, L.; Zhang, Y. B.; Li, T. S.; Kim, J.; Chim, C.; Galli, G.; Wang, F. *Nano Lett.* **2010**, *10*, 1271.
(10) Banerjee, S.; Richardson, W.; Coleman, J.; Chatterjee, A. *Electron Dev. Lett.* **1987**, *8*, 347.
(11) Coleman, J. N.; et al. *Science* **2011**, *331*, 568.
(12) Jelle, B. P.; Breivik, C.; Røkenes, H. D. *Sol. Energy Mater. Sol. Cells* **2012**, *100*, 69.
(13) Hybertsen, M. S.; Louie, S. G. *Phys. Rev. Lett.* **1985**, *55*, 1418.
(14) Cahangirov, S.; Topsakal, M.; Aktürk, E.; Şahin, H.; Ciraci, S. *Phys. Rev. Lett.* **2009**, *102*, 236804.
(15) Vogt, P.; De Padova, P.; Quaresima, C.; Avila, J.; Frantzeskakis, E.; Asensio, M.; Resta, A.; Ealet, B.; Le Lay, G. *Phys. Rev. Lett.* **2012**, *108*, 155501.
(16) Fleurence, A.; Friedlein, R.; Ozaki, T.; Kawai, H.; Wang, Y.; Yamada-Takamura, Y. *Phys. Rev. Lett.* **2012**, *108*, 245501.
(17) Chen, L.; Liu, C.-C.; Feng, B.; He, X.; Cheng, P.; Ding, Z.; Meng, S.; Yao, Y.; Wu, K. *Phys. Rev. Lett.* **2012**, *109*, 056804.
(18) Kunstmann, J.; Quandt, A. *Phys. Rev. B* **2006**, *74*, 035413.
(19) Lau, K. C.; Pandey, R.; Pati, R.; Karna, S. P. *Appl. Phys. Lett.* **2006**, *88*, 212111.
(20) Liu, C. C.; Feng, W. X.; Yao, Y. G. *Phys. Rev. Lett.* **2011**, *107*, 076802.
(21) Ezawa, M. *Phys. Rev. B* **2012**, *86*, 161407.
(22) Feng, B. J.; Ding, Z. j.; Meng, S.; Yao, Y. G.; He, X. Y.; Cheng, P.; Chen, L.; Wu, K. H. *Nano Lett.* **2012**, *12*, 3507.
(23) Meng, L.; Wang, Y. L.; Zhang, L. Z.; Du, S. X.; Wu, R. T.; Li, L. F.; Zhang, Y.; Li, G.; Zhou, H. T.; Hofer, W. A.; Gao, H. J. *Nano Lett.* **2013**, *13*, 685.
(24) Guo, Z. X.; Furuya, S.; Iwata, J.; Oshiyama, A. *Phys. Rev. B* **2013**, *87*, 235435.
(25) Guo, Z. X.; Furuya, S.; Iwata, J. I.; Oshiyama, A. *J. Phys. Soc. Jpn.* **2013**, *82*, 063714.
(26) Guo, Z. X.; Oshiyama, A. *Phys. Rev. B* **2014**, *89*, 155418.
(27) Wang, Y.; Lv, J.; Zhu, L.; Ma, Y. *Phys. Rev. B* **2010**, *82*, 094116.
(28) Wang, Y.; Lv, J.; Zhu, L.; Ma, Y. *Comput. Phys. Commun.* **2012**, *183*, 2063.
(29) Kennedy, J.; Eberhart, R. *Proceedings of the IEEE International Conference on Neural Networks*; IEEE: Piscataway, NJ, 1995; Vol. *4*, p 1942.
(30) Wang, Y.; Miao, M.; Lv, J.; Zhu, L.; Yin, K.; Liu, H.; Ma, Y. *J. Chem. Phys.* **2012**, *137*, 224108.
(31) Blöchl, P. E. *Phys. Rev. B* **1994**, *50*, 17953.
(32) Kresse, G.; Hafner, J. *Phys. Rev. B* **1994**, *49*, 14251.
(33) Perdew, J. P.; Zunger, A. *Phys. Rev. B* **1981**, *23*, 5048.
(34) Ceperkey, D. M.; Alder, B. *J. Phys. Rev. Lett.* **1980**, *45*, 566.
(35) Heyd, J.; Scuseria, G. E.; Ernzerhof, M. *J. Chem. Phys.* **2003**, *118*, 8207.
(36) Parlinski, K.; Li, Z. Q.; Kawazoe, Y. *Phys. Rev. Lett.* **1997**, *78*, 4063.
(37) Togo, A.; Oba, F.; Tanaka, I. *Phys. Rev. B* **2008**, *78*, 134106.
(38) Slater, J. C. *J. Chem. Phys.* **1964**, *41*, 3199.
(39) Huang, B.; Deng, H. X.; Wei, S. H. *Phys. Rev. X* **2014**, *4*, 021029.

(40) Gimbert, F.; Lee, C. C.; Friedlein, R.; Fleurence, A.; Yukiko, Y.; Ozaki1, T. arXiv:1401.0142.
(41) Perdew, J. P.; Burke, K.; Ernzerhof, M. *Phys. Rev. Lett.* **1996**, *77*, 3865.
(42) Xiang, H. J.; Kan, E. J.; Wei, S. H.; Whangbo, M.-H.; Yang, J. L. *Nano Lett.* **2009**, *9*, 4025.
(43) Huang, B.; Xiang, H. J.; Xu, Q.; Wei, S. H. *Phys. Rev. Lett.* **2013**, *110*, 085501.
(44) Xiang, H. J.; Kan, E. J.; Wei, S. H.; Gong, X. G.; Whangbo, M.-H. *Phys. Rev. B* **2010**, *82*, 165425.
(45) Xiang, H. J.; Wei, S.-H.; Gong, X. G. *Phys. Rev. B* **2010**, *82*, 035416.
(46) Xiang, H. J.; Huang, B.; Kan, E.; Wei, S. H.; Gong, X. G. *Phys. Rev. Lett.* **2013**, *110*, 118702.